# Mechanics of Non-Uniform Grid Shell Structures

Kumil Ali

December 15, 2022

Submitted to

Stony Brook University

in partial fulfillment of the requirements for the degree of

Civil Engineering - Master of Science

Advisor: Dr. Paolo Celli

# Contents

# 1 Introduction and Background

## 1.1 Introduction

Some biological but commonly used construction materials such as wood and bamboo are examples of materials in which samples, even in similar populations, could have vastly different structural and mechanical properties. Unlike steel or concrete, the unique growth conditions and other parameters unique to an individual tree or culm. Many societies have used these materials for all matters of construction and tools, and this is unlikely to change over time. With a climate crisis looming, sustainability is an ever-growing concern, and the need for sustainable architecture utilizing renewable construction materials is ever more necessary. The variance in elements made of these materials can be made suitable to modern construction practices with developments in new structural engineering techniques. In particular, the utilization of Grid Shell structures can better take advantage of these materials for use in a more sustainable structures.

Grid Shell structures are planar networks composed of rod-shaped elements, that when loaded laterally along the network edges, "pop up" into shell structures [1]. The "pop up" of grid shell structures refer to the actuation of the planar network into a 3D target configuration. Due to this unique dynamic property, Grid Shells can provide structural engineers and architects the ability to design structures with large spans without the need of columns. Due in part to the complexity of grid shell designs, each design must be analyzed on a case-by-case basis [2].

Grid shells generally utilize elastic rods and contain uniform members and joints, with special emphasis placed on overall smoothness of design [3]. The joints connecting the elastic rods must be capable of in-plane rotation, which in turn allow large deformations upon loading. For engineers, and architects creating the grid shell require an understanding of the grid lengths, boundary conditions, and grid patterns needed to attain an appropriately performing design. Research has and is being done that would target specific 3D actuated forms with unique loading and boundary conditions. Utilizing materials such as bamboo and wood which have varying mechanical properties introduces a new consideration for architects, and engineers. A large portion of the research pertaining to grid shells focus exclusively on the mechanics of uniform grid shells, adding non-uniform materials such as bamboo add an extra layer of complexity to the overall understanding of how grid shells behave. This paper will try to understand the mechanics of non-uniform grid shell structures.

## 1.2 Literature Review

Unlike many traditional structures like plates, which are often composed of solid homogeneous or composite materials, Grid shells, evident by the name, are composed of grids of linear rods of varying materials. Consequently, each grid can be triangular, rectangular, or any other shapes that may be appropriate for the design [4].

Grid shell structures are often composed of discrete members that are lightweight and can carry loads efficiently [4]. Suitable materials include steel, aluminum, wood, bamboo and many others. Grid shells are also more efficient and can lower the operating energy needed for construction due to its lower demand for materials [5].

Research for grid shells has been conducted since the 1970s, and various forms of grid shells have been developed and studied by researchers. However, due to the unique form of each grid shell structure, research considerations have focused on one set of standard grid shells, albeit with slight modifications in boundary conditions, loads, and initial configurations. One such example is a new sub-field of grid shells known in the community as X-shells or de-ployable structures. The beams utilized in these special shells are elastically deformable and have rotational joints [6]. One of the features differentiating X-shells would be it foregoing conventional assemblages of flat grid shells

and would instead introduce irregular planar grids with pre-developed torque on certain joints. This research would help to understand the behavior of grid shells when intrinsically actuated.

Other forms of research take into account hybrid grid shells which are made of pre-tensioned quadrangular meshes that are coupled with cable nets. The objective of the research seeks to understand the impact of asymmetrical loads on the elasto-plastic buckling capacity of the hybrid grid shell structure [7]. It is mentioned that the scaling of the imperfection needed for post-buckling analysis is as important as the shape, and by performing an imperfection analysis a proper understanding of the buckling capacity of a structure can be realized.

In addition, to research specific grid shell designs, numerous tools have been developed such as the NURBS interpretation that would help understand the role of curvature in grid shell design. Newer research is focused on incorporating natural materials like bamboo into the grid shell design. Due to the anisotropic and non-homogeneous material properties of bamboo, the research focuses exclusively on isotropic, and homogeneous bamboo compositions and the utilization of bamboo in developing unique arch designs for outdoor infrastructure [8]. New research is continually being brought forth that will enhance our fundamental knowledge of grid shell structures.

### 1.3 Objectives

The goal of this experiment was to initially focus on Non-Uniform grid shell structures due to the lack of comprehensive research on its mechanics. This paper will instead take a step towards modelling non-uniformity by developing a comprehensive understanding of the mechanics of uniform grid shell structures. This paper will focus on learning grid shell behavior by modeling experimentally and numerically using non-linear simulations in ABAQUS.

### 1.4 Inspiration and Motivation

Grid Shells are structures that can have varying forms depending on the loads and displacements that its extremities are subjected to. This paper will seek to develop an understanding of the forces required to actuate a grid shell and understand the mechanics of grid shell behavior. The inspiration to the grid shell structure was drawn by a paper done by Baek et.al [1]. The paper developed a physical table top prototype as shown in Figure 1. The anatomy and actuation of the grid shell utilized in the experimental and numerical portion of this paper utilized the same properties as discussed in the paper. Our experiment will seek to replicate the experiment done by Baek and create the model experimentally and numerically.

### 1.5 Procedural Outline

In Section 2, our experimental approach and set up will be discussed, including a comprehensive review of the various properties and elements utilized by Baek et al. in the development of his table-top prototype. The various methodologies and experimental results will be discussed prior to the introduction of the numerical analysis. In Section 3, a numerical model developed in ABAQUS will introduce the process of assembly, selection of joints, and the use of Linear Buckling Analysis and Post-Buckling Analysis, along with a comprehensive review of the computational parameters. The results and validation steps will be discussed in Section 4 to gauge the effectiveness of the experimental and numerical model. The 5th section will conclude our analysis with a discussion on future research.

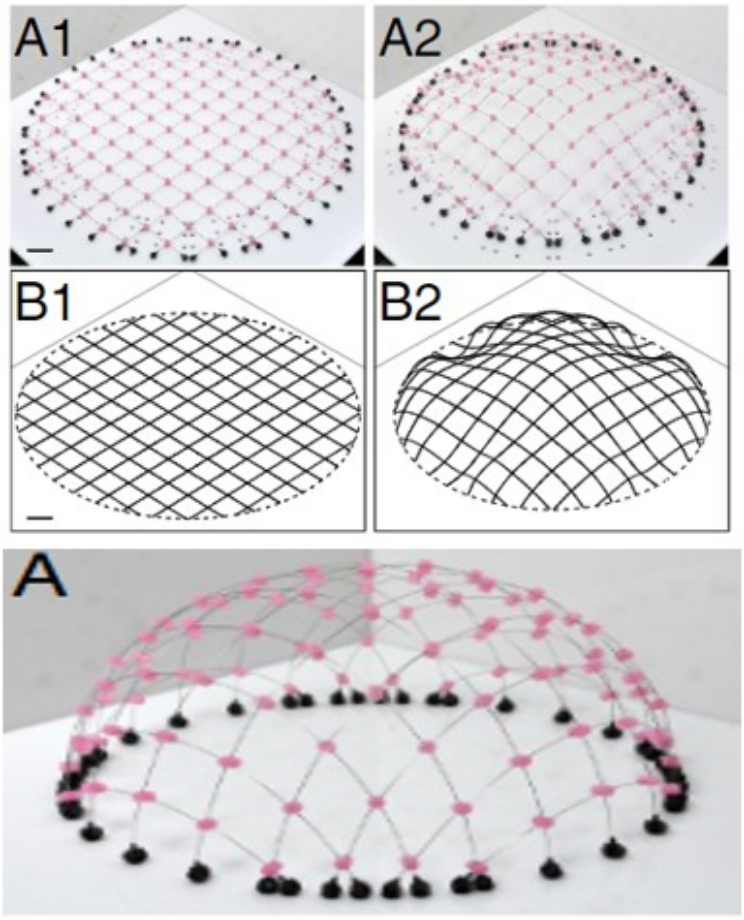


Figure 1: Table-Top Prototype Inspiration

## 2 Experimental Model

### 2.1 Experimental Set up

The experimental set-up replicated the anatomy and actuation of the table-top model designed by Baek et al. To be concise, a simple description of the setup will be briefly discussed. First, a sheet of acrylic (depth = 500 $\mu$m) was laser cut into a series of square grids (spacing = 20 mm) with circular holes being cut at its intersections ($D_r$ = 3 mm). A circular footprint (D = 252 mm) was laser cut to serve as the boundary. Second, a set of Nitinol Rods were placed on the laser-cut grooves placed perpendicularly on top of one another, the properties of the Nitinol rods ($D_r$ = 254 $\mu$m) are as follows:

| | |
|---|---|
| Young's Modulus, $E$ | 83 GPa |
| Poisson's ratio, $\nu$ | 0.3 |

These values were also utilized for the numerical model on ABAQUS. After the assembly of the nitinol rods onto the laser-cut grooves, Silicon rubber mold was applied at each joint to allow the joining of the rods and allow in-plane rotation. Additionally, circular holes ($D_h$ = 4 mm) were laser-cut in the acrylic at the location of the edges of each nitinol rod. These circular holes would serve as the boundary node location. A slight modification to Baek's model was made with respect

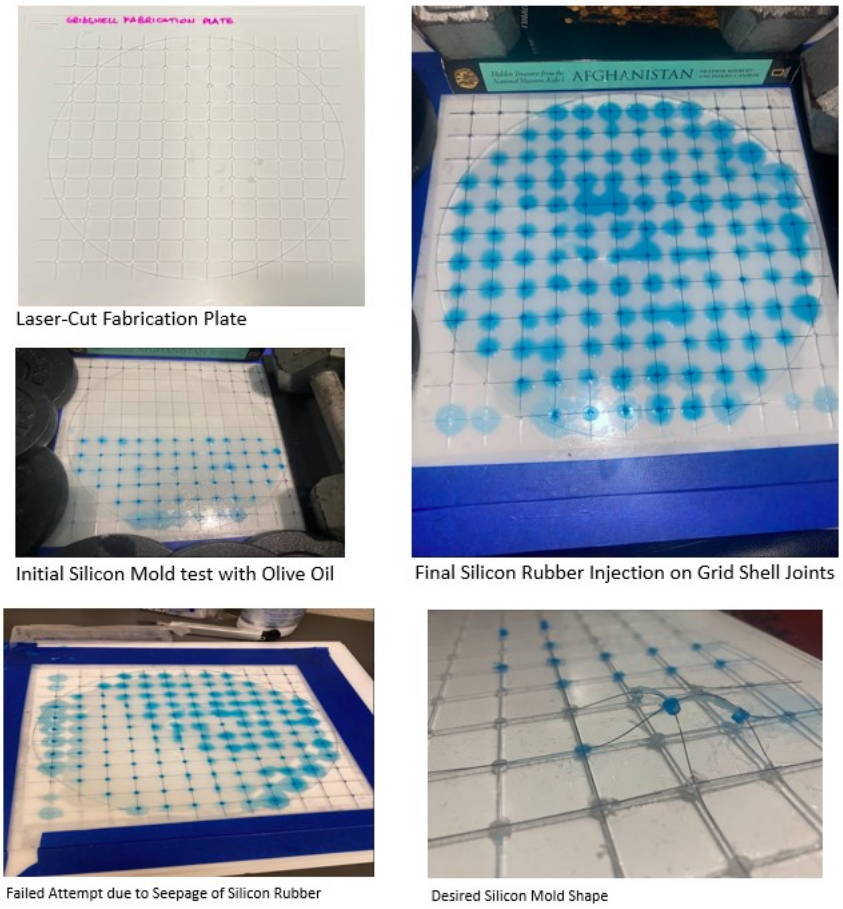


Figure 2: Fabrication Setup and Trials

to the boundary nodes, in lieu of 3D printed ball joints ($D_r = 4$ mm), Styrofoam ball joints were utilized due to fabrication difficulties and were manually fitted into the edges of nitinol rods in the location of the circular holes. Finally, to prevent the separation and lateral movement of beam elements (nitinol rods) small traces of super glue were applied at the edge of each silicon joint, and on the boundary nodes.

A key detail in the fabrication process involved the use of a mixture of Olive Oil and WD-40 to prevent seepage of the Silicon Rubber during assembly. Images of the fabrication process are shown in Fig. 2. Another Fabrication plate was laser cut to an actuated boundary of $R_a = 115.9$ mm.

## 2.2 Experimental Results

With the development of the grid shell complete, a gradual force was applied to all boundary nodes until the grid shell compressed to the circular actuated boundary of $R_a = 115.9$ mm from the original boundary. As the grid shell was compressed with the movement of the boundary ball joints to the inner boundary, the height of the mid-section increased and a dome-shaped grid shell appeared. The actuated grid shell is shown in Fig. 3. From the actuation of the grid shell it appears the dome-shaped grid shell follows a flattened dome pattern at its center nodes.

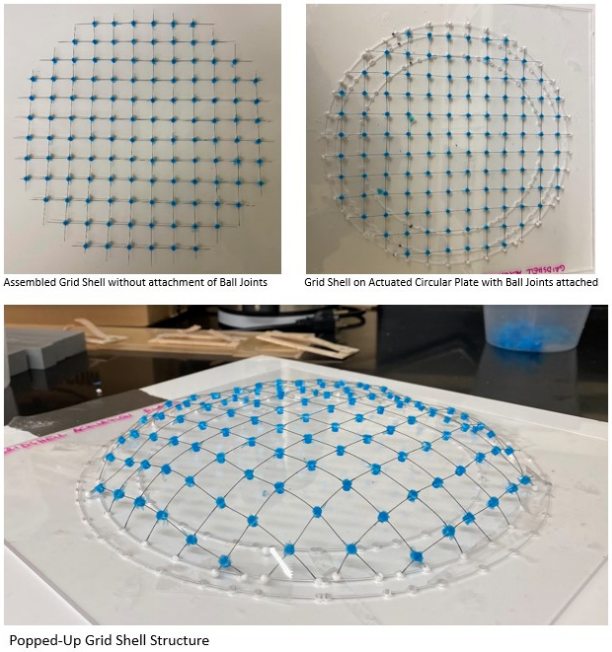


Figure 3: Actuation of the Grid Shell to prescribed inner boundary

# 3 Numerical Analysis

## 3.1 Beam and Joint Selection

To properly develop a numerical model, various tests were conducted to determine the ideal beam and joint configuration. Beam elements would be utilized with the same properties mentioned in Sections 2.1. After careful analysis of the literature, beam element B31H was ultimately chosen (2-node linear beam with hybrid formulation). A B31H beam element was chosen due to its unique approach in solving geometrically nonlinear structures that undergo large rotations. Additionally, this formulation allows faster convergence and utilizes a much more efficient method over classical finite element theory approaches [9].

To design the hinges, 2 approaches were made to connect the beam members and allow rotation relative to one another. The first approach as shown in Fig. 4 utilizes a tie constraint that would connect the 2 members in question at its intersection and allow a rotation between one another. The trial was conducted on a sample 20 mm x 20 mm cross-section to replicate our grid shell. With out-of plane movement restricted on all nodes, our deformed shape indicates that while member connection is achieved, rotation between members does not occur.

The second approach utilizes a Pin (Hinge) Joint as shown in Fig. 5. To model the hinge joint accurately, special considerations were made with respect to the in-plane rotational stiffnesses: $D_{44}$ and $D_{55}$ which has a value of $1 \cdot 10^4 N \cdot m/rad$, and the out-of plane rotational stiffness, $D_{66}$ which has a value of $1 \cdot 10^{-2} N \cdot m/rad$. These values were obtained through a convergence test which will be discussed in detail in Sections 3.2.3. The same trial was conducted on this Pin Joint on the 20 mm x 20 mm cross section, the deformed shape generated revealed that rotation between members occur. Our numerical analysis would utilize this Pin Joint as our connection.

```
v1 = a.instances['Part-6-1'].vertices
verts1 = v1.findAt(((-10.0, -10.0, 0.0), ))
region2=a.Set(vertices=verts1, name='s_Set-1')
mdb.models['Model-1'].Tie(name='Constraint-1', master=region1, slave=region2,
    positionToleranceMethod=COMPUTED, adjust=ON, tieRotations=ON,
    thickness=ON)
a1 = mdb.models['Model-1'].rootAssembly
a1.translate(instanceList=('Part-G-1', ), vector=(-406.992, 0.0, 0.0))
a = mdb.models['Model-1'].rootAssembly
v1 = a.instances['Part-G-1'].vertices
verts1 = v1.findAt(((-125.6, -10.0, 0.0), ))
region = a.Set(vertices=verts1, name='Set-3')
```

Generic Code Snippet of the Tie Constraint generated in Python

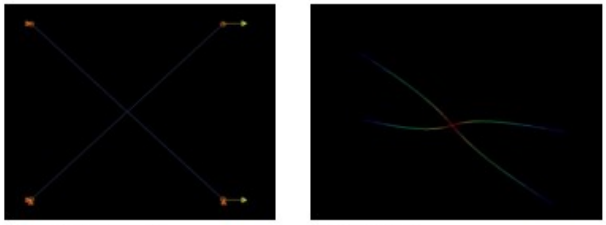

Rigid Tie Constraint Joint | Deformed Shape

Figure 4: Rigid Joint Code and Assembly

```
a.Set(edges=edges1, name='Wire-1-Set-1')
mdb.models['Model-1'].ConnectorSection(name='ConnSect-1',
    translationalType=JOIN, rotationalType=ROTATION)
elastic_0 = connectorBehavior.ConnectorElasticity(components=(4, 5, 6), table=(
    (10000.0, 10000.0, 0.1), ))
mdb.models['Model-1'].sections['ConnSect-1'].setValues(behaviorOptions =(
    elastic_0, ) )
mdb.models['Model-1'].sections['ConnSect-1'].behaviorOptions[0].ConnectorOptions(
    )
a = mdb.models['Model-1'].rootAssembly
e1 = a.edges
edges1 = e1.findAt(((75.106844, -0.01, 0.0), ))
region=a.Set(edges=edges1, name='Set-2')
csa = a.SectionAssignment(sectionName='ConnSect-1', region=region)
```

Generic Code Snippet of the Hinge Constraint generated in Python

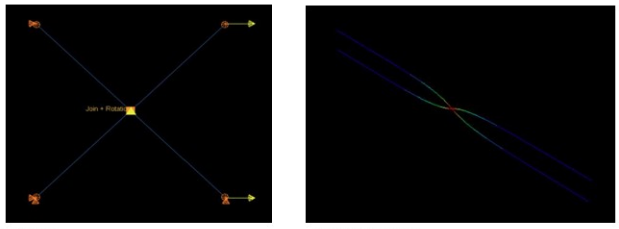

Pin Joint | Deformed Shape

Figure 5: Pin Joint Code and Assembly

### 3.2 Grid Shell Assembly

The Grid Shell assembly was developed through ABAQUS and was assembled element by element, with Pin Joint conditions applied to all intersections between beam elements. The properties mentioned in Section 2.1 and 3.1 were applied to the numerical model. The geometry of the grid shell is shown in Fig. 6. As shown in Fig. 6, Point A will be used to measure the magnitude of displacement at that point along with the force applied relative to that point. Point B will be used to measure the out-of plane displacement at that point, these points were chosen as they can be measured numerically in ABAQUS and experimentally measured.

At each boundary node on the grid shell, a reference force magnitude ($F_r = 1$) was applied, this force was broken into its $x$ and $y$ components as the force would be applied radially. Additionally, the out-of plane displacement ($U_3$) was blocked as the grid shell would only be compressed along the $x$ and $y$ directions. Additional pins were placed along the outer-central boundary nodes to enable the grid shell to buckle under the forces applied. The corresponding Boundary conditions

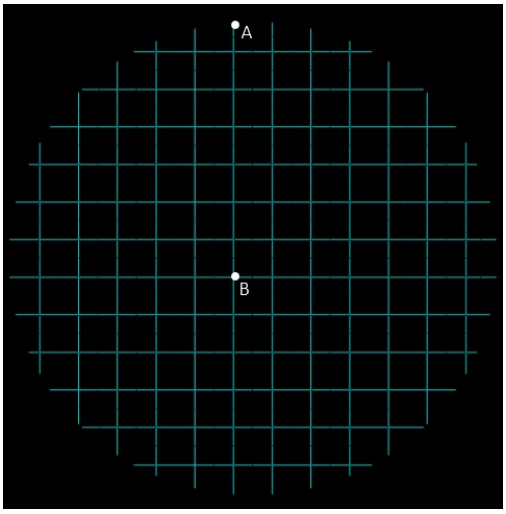


Figure 6: Grid Shell Geometry

and loads applied are shown in Fig. 7.

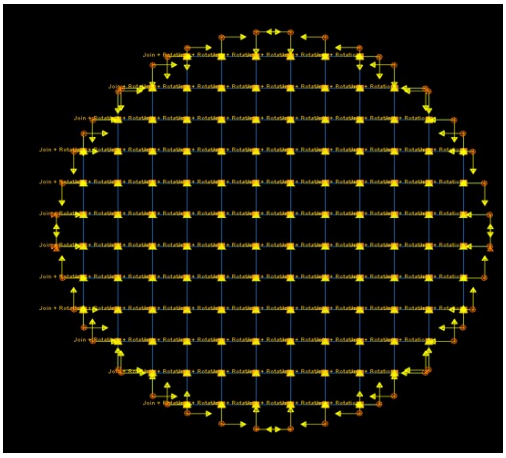

Figure 7: Boundary Conditions and Loads Applied

### 3.2.1 Linear Buckling Analysis

Due to the Geometric non-linearity inherently present in grid shells, out-of-plane buckling will occur. As a result linear buckling analysis is applied to our numerical model. This would help verify that the grid shell would behave and buckle in a similar fashion to our experimental model. Additionally, the linear buckling analysis performed on ABAQUS would generate various mode shapes that would provide a general idea on the buckled shape of the grid shell, as well as an eigenvalue that would be utilized during post-buckling analysis. In our analysis, mode shape 1, shown in Fig. 8 closely aligned with the general shape our experimental model yielded, and an eigen value of $2.716 \cdot 10^{-3}$ was generated.

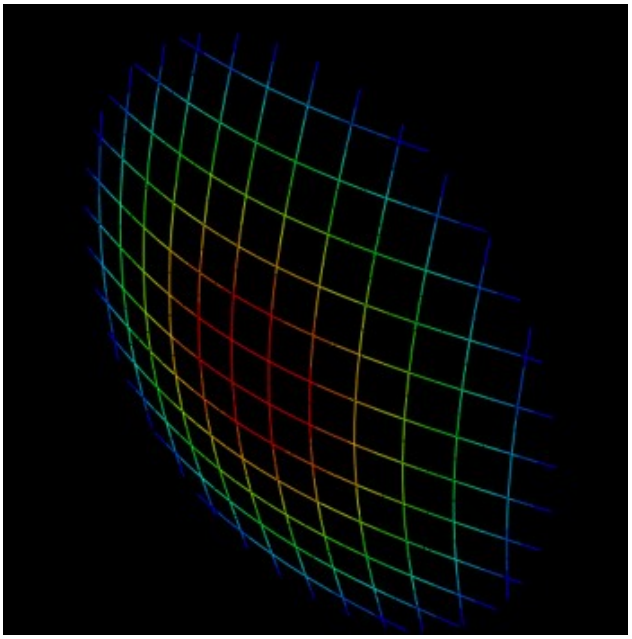

Figure 8: Linear Buckling Analysis - Shape of Mode 1

### 3.2.2 Post-Buckling Analysis

Post-Buckling analysis is typically performed after buckling analysis to understand how a structure will likely fail when the load application is high [10]. The buckling mode obtained from the linear buckling analysis would typically serve as the imperfection that is applied to the structure prior to the start of post-buckling. An imperfection of $2 \cdot 10^{-7}$ was ultimately applied to the structure based on an imperfection analysis which is explained in Sections 3.2.3. This imperfection is utilized to push our structure to buckle as intended. Utilizing the eigen value generated from the linear buckling analysis as a load factor, the load factor would be multiplied by the initial reference force magnitude ($F_r = 1$) to obtain the critical load needed for post-buckling analysis.

### 3.2.3 Convergence Tests

As discussed in sections 3.1 and 3.2.2, various convergence tests were performed to obtain the mesh density, imperfection needed for post-buckling analysis, and the $D_{44}$, $D_{55}$, and $D_{66}$ values. Convergence tests are typically performed to find the ideal value of a chosen parameter, through multiple iterations and data points being generated, an ideal value would be selected upon convergence to a fixed value (plateau). The ideal value for our series of convergence tests would be the out-of plane displacement at Point A in Fig. 6. The results generated from the convergence tests are shown in Fig. 9 to Fig. 11.

Based on the results in Fig. 9, the mesh density of global size 0.01 ($L_x/100$) was selected. As the mesh of the model became finer, the out-of plane displacement values plateau, which indicate that any increase in the number of elements will generate similar out-of plane displacements as the less-fine mesh density size 0.01.

Based on the results in Fig. 10, the Imperfection value was selected as $2 \cdot 10^{-7}$. This result was chosen due to the out-of plane displacement values converging near $2 \cdot 10^{-7}$, any imperfection higher than the value selected does not seem to converge.

A convergence test was performed for the Out-of-Plane Rotational Stiffness, $D_{66}$. Based on

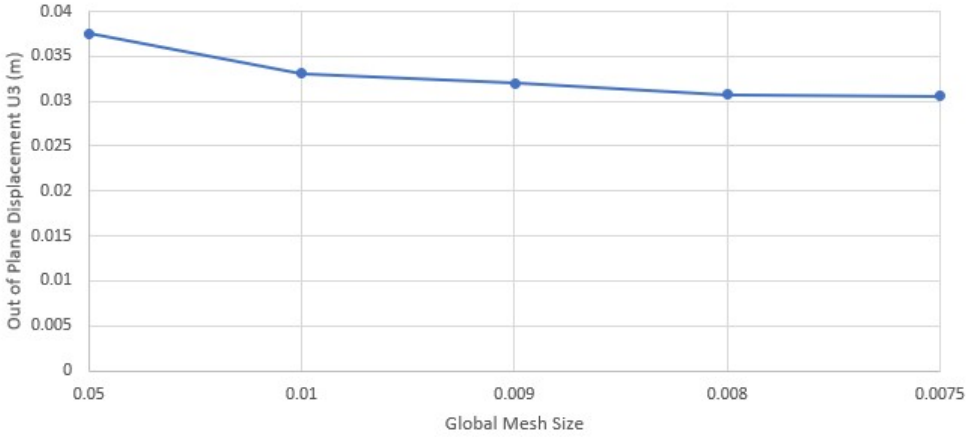


Figure 9: Mesh Density Convergence Test

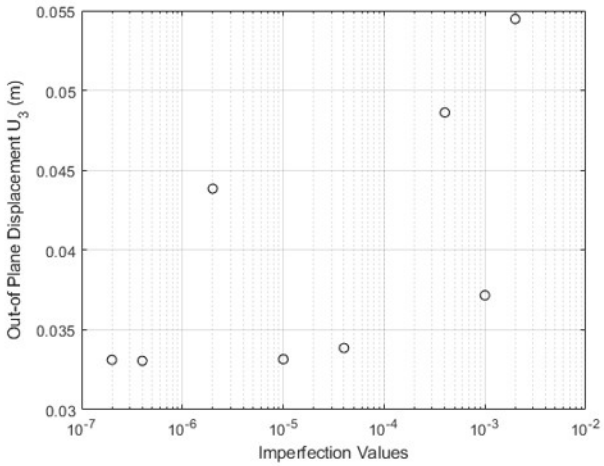


Figure 10: Imperfection Analysis Test

the results in Fig. 11, the $D_{66}$ seems to converge near the value $1 \cdot 10^{-2} N \cdot m/rad$ where the displacement values seem to plateau as the value of $D_{66}$ increases. A similar convergence test could be performed for the in-plane rotational stiffnesses $D_{44}$ and $D_{55}$, however the main goal of applying a value of $1 \cdot 10^{4} N \cdot m/rad$ was to have a large rotational stiffness to prevent rotation relative to $x$ and $y$.

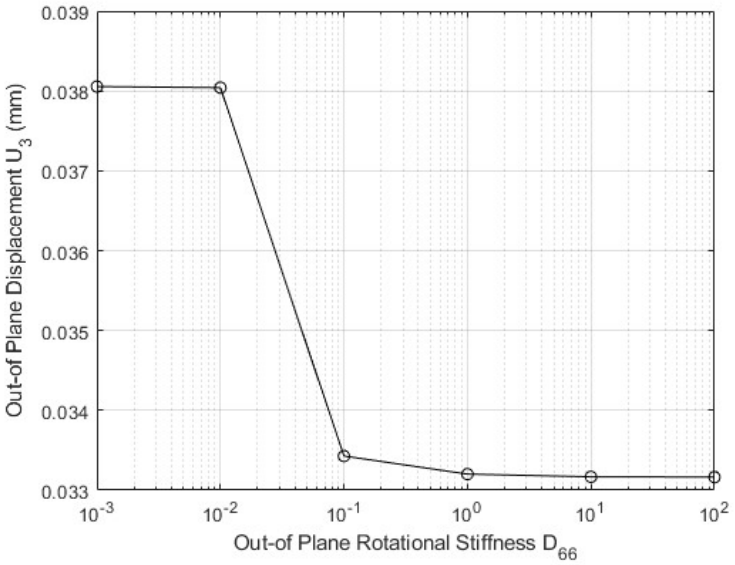


Figure 11: Out-of-Plane Rotational Stiffness, $D_{66}$ Convergence Test

# 4 Results

## 4.1 Observations

Our numerical results were generated through a careful layer of steps that involved performing a Linear Buckling Analysis, identifying the most appropriate mode shape, and utilizing the Eigen-Value of that respective mode to calculate the critical loads to be applied to the Post- Buckling Analysis step. The ultimate goal of the numerical model in ABAQUS was to apply a force that would compress the grid shell into the actuated boundary of $R_a = 115.9$ mm. Applying a $F_{critical}$ = (Eigen-Value)*($F_r = 1$) to our post-buckled shape, it is quickly determined that the grid shell does not compress to the actuated boundary, and as a result a load increment, n would need to be applied to $F_{critical}$ in order to compress the grid shell to the intended boundary. An initial increment of n = 5 was selected to see whether the grid shell would compress to the intended boundary. Several plots were generated for the n = 5 increment, one of the plots generated as shown in Fig. 12 is the Displacement Magnitude at Point A vs. Out-of Plane Displacement at Point B plot (Points A and B are highlighted in Fig. 7). Analyzing the plot generated indicates that at the beginning our grid shell does not pop-up, but with a steady increase in displacement magnitude our system begins to pop up. However, upon further inspection, the displacement magnitude at Point A falls short of the 10.1 mm displacement needed to fit into the actuated boundary of $R_a = 115.9$ mm. An increase in the load increment is necessary.

Another plot generated is the force displacement as shown in Fig. 13, this plot describes the behavior of the grid shell structure. Initially, the force displacement plot shows a very steep line which indicates a high stiffness in the structure, however with the application of a very small displacement magnitude applied at the boundary nodes, the grid shell structure exhibits a softening behavior and an overall loss of stiffness in the system. This result verifies our initial understanding of the Post-Buckling analysis of a beam, as a bi-linear system would ensue, as initially the grid shell structure is very stiff, but when buckling begins the system becomes weaker.

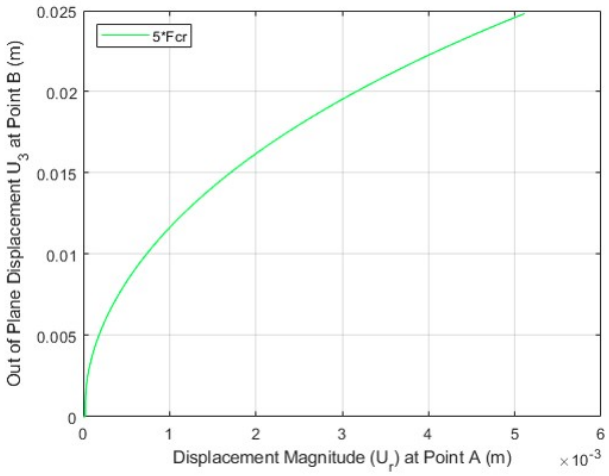


Figure 12: Displacement v. Displacement Plot for F = $5 \cdot (F_{critical})$

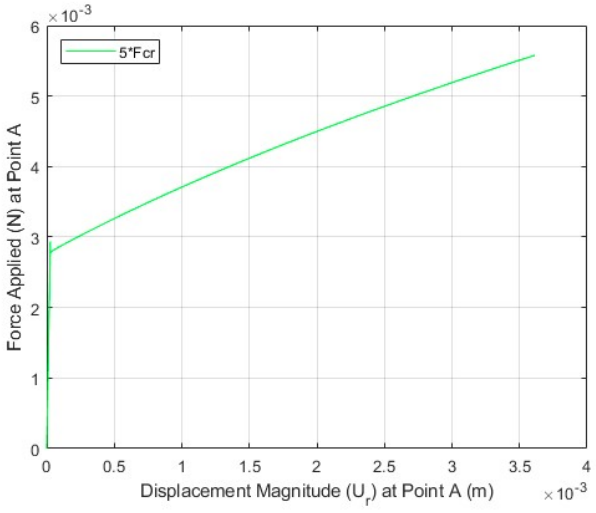


Figure 13: Force v. Displacement for F = $5 \cdot (F_{critical})$

## 4.2 Validation

A larger simulation was run for a force, F = $12.5 \cdot (F_{critical})$ applied on the boundary nodes of the grid shell. Upon investigation, the results generated by the larger simulation check out with the results generated by the experimental model. In the force displacement plot as shown in Fig. 14, we exhibit similar behavior as seen in Fig 13 for F = $5 \cdot (F_{critical})$, our grid shell structure is initially very stiff, but experiences a gradual loss of stiffness upon buckling. The Displacement Magnitude at Point A vs. Out-of Plane Displacement at Point B plot was also generated as shown in Fig. 15. Analyzing the results, it is seen that a steady increase in the displacement magnitude causes the grid shell to pop-up. Looking at the displacement magnitude of 10.1 mm at Point A, which is the same displacement needed to actuate our grid shell, an out-of plane displacement is recorded at around 33.5 mm. Additionally, the error bar placed in Fig. 15 signifies where the model should displace and the out-of plane displacement relative to that point which further validates our analysis.

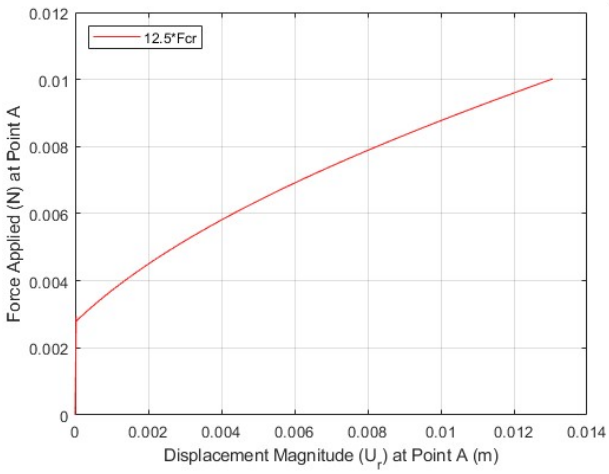


Figure 14: Force v. Displacement Plot for F = $12.5 \cdot (F_{critical})$

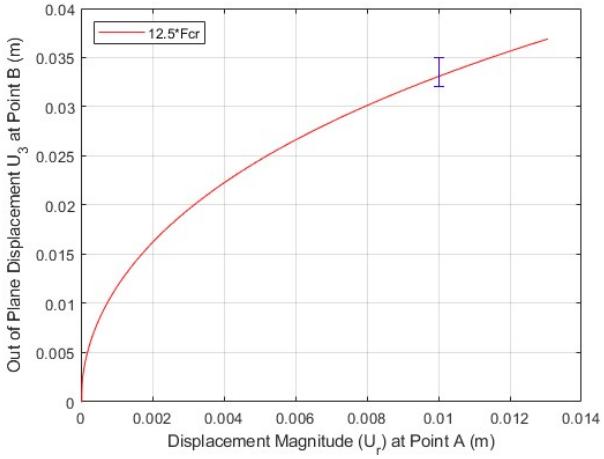


Figure 15: Displacement v. Displacement Plot for F = $12.5 \cdot (F_{critical})$

Additionally, a small check was performed by super-imposing Figs. 13 and 14 along with Figs. 12 and 15. The results are shown in Fig. 16 and Fig. 17, where it is shown that the increment choice affects convergence but does not alter the results.

### 4.3 Displacement Profiles

To further validate the results, a displacement profile was developed to compare the out-of plane displacements of the experimental and numerical model. The results were generated by taking the out-of plane displacements for Points 1 to 12 as shown in Fig. 18 in the numerical model and by experimentally measuring the out-of-plane displacements utilizing a caliper. Observing the general profile of the experimental and numerical model, both displacement profiles generally align with respect to one another.

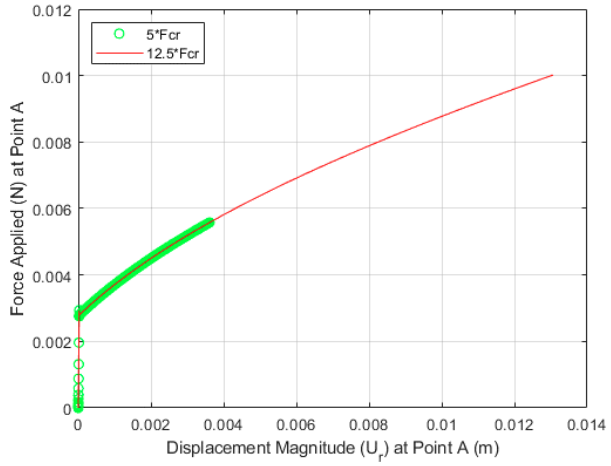


Figure 16: Force v. Displacement Validation Check

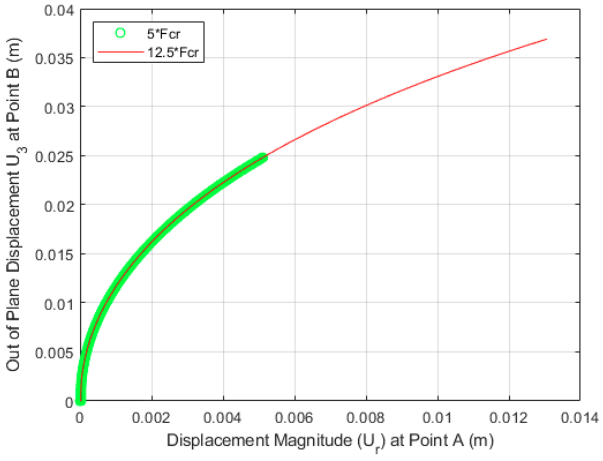


Figure 17: Displacement v. Displacement Validation Check

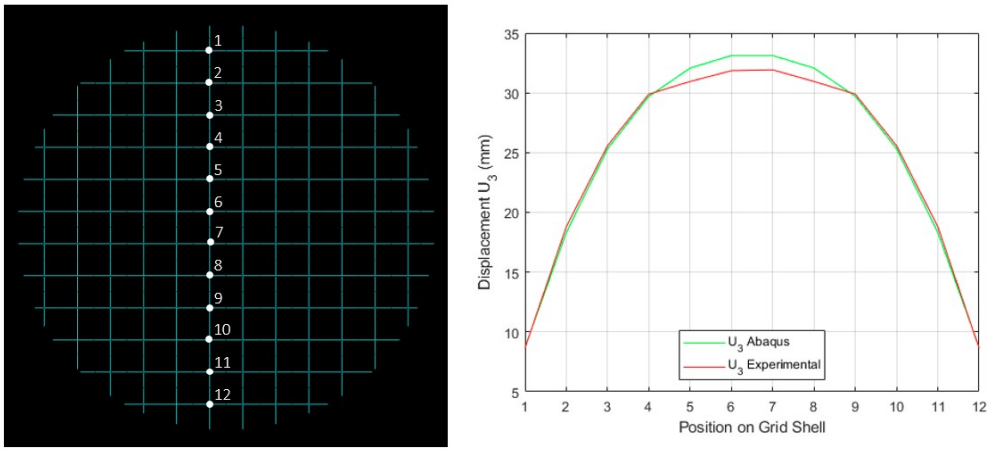


Figure 18: Displacement Profiles

# 5 Conclusion and Future Work

The results generated by the experimental and numerical models were conclusive and established an understanding of the mechanics of uniform grid shell structures. By performing both experimental and numerical analysis, we were able to validate our results. In the experimental model, gradually compressing a flat grid shell structure at its extremities, actuated the flat grid shell into a shell shaped structure. This result was later validated by designing a numerical model to replicate the physical behavior of a grid shell. Through complex non-linear analysis and refinement of various model parameters, our numerical model almost perfectly replicates the experimental setup. The results generated also further enforce a general understanding of beam and grid shell structures. Grid shell structures are initially very stiff, but with an application of force and the start of buckling, the stiffness begins to soften and decrease which reinforces research done on the post-buckling analysis of beams which follow a similar path.

While, the initial parameters of this research involved understanding the mechanics of non-uniform grid shells, the analysis was ultimately made for a uniform grid shell model which is a step towards understanding the mechanics of non-uniform grid shell structures. Given the fluidity of the python code generated through ABAQUS, these simulations can be extended towards non-uniform structures. The shape of the grid shell can also be modified to understand how the shape of the planar network of rods behave when subjected to forces in its boundaries and how they buckle in response.

Since the structure presented in this research is defined by preset conditions and parameters, an infinite number of grid shells with uniform and non-uniform properties can be explored. While the analysis replicated the table-top experiment done by Baek et al, this experiment can be expanded and scaled, and further research can be conducted on how the results would vary depending on the overall scale of the model. The future work needed to understand the mechanics of non-uniform grid shells is limitless, in addition to the considerations mentioned above, further research can explore the mechanics of woven non-uniform grid shells as well as the introduction of imperfections.

## References


[1] Baek, C., Sageman-Furnas, A. O., Jawed, M. K., & Reis, P. M. (2017). Form finding in Elastic gridshells. Proceedings of the National Academy of Sciences, 115(1), 75–80. https://doi.org/10.1073/pnas.1713841115

[2] Paoli, C. (C. A. (1970, January 1). Past and future of Grid Shell Structures. Past and future of grid shell structures. https://dspace.mit.edu/handle/1721.1/39277

[3] Form-finding of grid shells with continuous elastic rods. (n.d.). https://d-nb.info/1058106341/34

[4] Grid Shell Systems. (n.d.). https://www.octatube.nl/en_GB/systems.html/systemitem/12-grid-shells

[5] Malek, Samar. (2012). The effect of geometry and topology on the mechanics of grid shells.

[6] EPFL, J. P., Panetta, J., Epfl, Profile, E. P. F. L. V., EPFL, M. K.-L., Konaković-Luković, M., EPFL, F. I., Isvoranu, F., SA, E. B. I., Bouleau, E., SA, I., Profile, I. S. A. V., EPFL, M. P., Pauly, M., Zurich, E. T. H., & Metrics, O. M. V. A. (2019, August 1). X-shells: A new class of deployable beam structures: ACM Transactions on Graphics: Vol 38, no 4. ACM Transactions on Graphics. https://dl.acm.org/doi/10.1145/3306346.3323040

[7] Cai, J., Xu, Y., Feng, J., & Zhang, J. (2012). Nonlinear stability of a single-layer hybrid grid shell - researchgate. https://www.researchgate.net/publication/269377272_Nonlinear_stability_of_a_single-layer_hybrid_grid_shell

[8] Lionel Du Peloux, Olivier Baverel, Jean-François Caron, Frédéric Tayeb. From shape to shell: a design tool to materialize freeform shapes using gridshell structures. Design Modelling Symposium Berlin, Sep 2013, Berlin, Germany. ffhal-01199030f

[9] Getting started with Abaqus (V6.6). (n.d.). https://classes.engineering.wustl.edu/2009/spring/mase5513/abaqus/docs/v6.6/books/gsa/default.htm?startat=ch04s01.html

[10] Post buckling analysis. Simuleon. (2018, December 5). https://www.simuleon.com/post-buckling-analysis/#:~:text=Post%20Buckling%20Behaviour%2C%20also%20known,very%20short%20amount%20of%20time.